

Birhythmicity, intrinsic entrainment, and minimal chimeras in an electrochemical experiment

Cite as: Chaos **31**, 091102 (2021); <https://doi.org/10.1063/5.0064266>

Submitted: 21 July 2021 • Accepted: 23 August 2021 • Published Online: 14 September 2021

 Juliane C. Wiehl,  Maximilian Patzauer and  Katharina Krischer

COLLECTIONS

 This paper was selected as an Editor's Pick



View Online



Export Citation



CrossMark

ARTICLES YOU MAY BE INTERESTED IN

[A reliable chaos-based cryptography using Galois field](#)

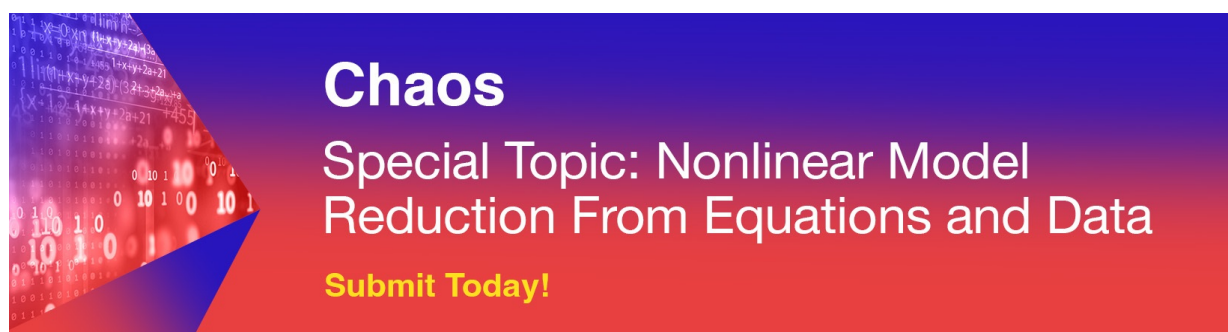
Chaos: An Interdisciplinary Journal of Nonlinear Science **31**, 091101 (2021); <https://doi.org/10.1063/5.0061639>

[Many-body quantum chaos and dual-unitarity round-a-face](#)

Chaos: An Interdisciplinary Journal of Nonlinear Science **31**, 093101 (2021); <https://doi.org/10.1063/5.0056970>

[Exponential distribution of lifetimes for transient bursting states in coupled noisy excitable systems](#)

Chaos: An Interdisciplinary Journal of Nonlinear Science **31**, 093105 (2021); <https://doi.org/10.1063/5.0059102>



Chaos
Special Topic: Nonlinear Model
Reduction From Equations and Data
Submit Today!

Birhythmicity, intrinsic entrainment, and minimal chimeras in an electrochemical experiment

Cite as: Chaos 31, 091102 (2021); doi: 10.1063/5.0064266

Submitted: 21 July 2021 · Accepted: 23 August 2021 ·

Published Online: 14 September 2021



View Online



Export Citation



CrossMark

Juliane C. Wiehl, , Maximilian Patzauer, , and Katharina Krischer^{a)} 

AFFILIATIONS

Nonequilibrium Chemical Physics, Department of Physics, Technical University of Munich, 85748 Garching, Germany

^{a)} Author to whom correspondence should be addressed: krischer@tum.de

ABSTRACT

The coexistence of limit cycles in a phase space, so called birhythmicity, is a phenomenon known to exist in many systems in various disciplines. Yet, detailed experimental investigations are rare, as are studies on the interaction between birhythmic components. In this article, we present experimental evidence for the existence of birhythmicity during the anodic electrodisolution of Si in a fluoride-containing electrolyte using weakly illuminated n-type Si electrodes. Moreover, we demonstrate several types of interaction between the coexisting limit cycles, in part resulting in peculiar dynamics. The two limit cycles exhibit vastly different sensitivities with respect to a small perturbation of the electrode potential, rendering the coupling essentially unidirectional. A manifestation of this is an asymmetric 1:2 intrinsic entrainment of the coexisting limit cycles on an individual uniformly oscillating electrode. In this state, the phase-space structure mediates the locking of one of the oscillators to the other one across the separatrix. Furthermore, the transition scenarios from one limit cycle to the other one at the borders of the birhythmicity go along with different types of spatial symmetry breaking. Finally, the master-slave type coupling promotes two (within the experimental limits) identical electrodes initialized on the different limit cycles to adopt states of different complexity: one of the electrodes exhibits irregular, most likely chaotic, motion, while the other one exhibits period-1 oscillations. The coexistence of coherence and incoherence is the characteristic property of a chimera state, the two coupled electrodes constituting an experimental example of a smallest chimera state in a minimal network configuration.

© 2021 Author(s). All article content, except where otherwise noted, is licensed under a Creative Commons Attribution (CC BY) license (<http://creativecommons.org/licenses/by/4.0/>). <https://doi.org/10.1063/5.0064266>

Bistability is both an interesting and a common phenomenon in dynamical systems.¹ The most common type of bistability is the coexistence of two stable stationary states. However, its meaning is more general and includes the coexistence of any two attractors in a phase space, such as of a stationary state and a limit cycle, of two limit cycles, and so on. Even bichaoticity, the coexistence of two chaotic attractors can occur. In this paper, we address an experimental system that exhibits the coexistence of two stable limit cycles, also referred to as birhythmicity. In a birhythmic system, each of the two coexisting stable oscillatory states can have its own frequency and amplitude and, in addition, might oscillate around different mean values.² While dynamic phenomena connected to the coexistence between two stationary states, such as transitions between them or traveling waves that might form in spatially extended systems, are well investigated,³ this is not the case for other types of bistability. Below, we demonstrate that the two directions of the transitions between the limit cycles can be of qualitatively different nature and that one oscillation might

intrinsically be influenced by the other coexisting limit cycle, a phenomenon we refer to as intrinsic entrainment. Furthermore, we show that the coupling between two birhythmic systems oscillating on different limit cycles can be strongly asymmetric.

I. INTRODUCTION

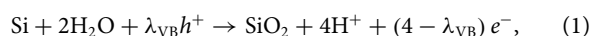
The discovery of birhythmicity in physical systems dates back to at least 1976 when it was reported to exist in a model of a continuous stirred tank reactor with consecutive exothermic reactions.⁴ To our knowledge, the first experimental finding of birhythmicity, then called generalized multistability by the authors, was reported in 1982 in a Q-switched gas laser.⁵ Later that year, Decroly and Goldbeter introduced the term birhythmicity in their theoretical study of a sequence of enzymatic reactions in a system with two positive feedback loops in series.² This was one of the first attempts to characterize birhythmicity in more detail. Their approach was later

used in an experimental study in which two chemical oscillators with a common intermediate were combined, and the resulting system was found to exhibit birhythmicity.^{6,7} Other examples of experimental chemical systems exhibiting birhythmicity include electronic oscillators,⁸ the Belousov–Zhabotinsky reaction in a stirred flow reactor,^{9–11} acetaldehyde oxidation in a continuously stirred tank reactor,¹² and the gas-phase $\text{H}_2 + \text{O}_2$ reaction in a continuously stirred tank reactor.^{13,14} Furthermore, birhythmicity proved to be important in diverse biological contexts, most notably neural activities, where examples for experimental evidences can be found, e.g., in Refs. 15–17, or circadian oscillators, where an experimental demonstration is reported in Ref. 18. More recently, an experimental electrochemical example of birhythmicity has been found in the oscillatory electrodisolution of Cu when using a delay feedback.¹⁹

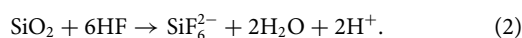
Compared to the relatively small number of experimental studies, the number of theoretical investigations on birhythmicity is much larger (see, e.g., references in Ref. 1). Besides models of ordinary differential equations describing specific systems, also generic properties of spatially extended birhythmic systems or coupled birhythmic oscillators have been studied with normal form type equations. These include wave phenomena in spatially extended reaction–diffusion models and ensembles of coupled birhythmic (phase) oscillators.^{20–27} The latter were also found to promote the occurrence of chimera states, an interesting prediction that awaits experimental validation.

In this paper, we investigate the nonlinear dynamics occurring during silicon electrodisolution in a fluoride-containing electrolyte. This system exhibits a plethora of dynamical phenomena, such as oscillations,^{28–30} phase clusters and chemical turbulence,³¹ and chimera states.³² Moreover, it has been found that the system exhibits two types of limit cycles, which were coined low amplitude oscillations (LAOs) and high amplitude oscillations (HAOs), respectively.³³ Although the electrochemical mechanism leading to either of these oscillations is not yet known, experiments suggested that they arise due to two different main feedback loops in the system.³³ Later, Tosolini *et al.* reported the coexistence of chaotic attractors and speculated that the bichaoticity is linked to an intrinsic birhythmicity, the interaction between the coexisting oscillators in the phase space causing both of the limit cycles to become unstable and give rise to chaotic attractors.³⁴ Here, we will continue on this path and show that the electrodisolution of silicon does indeed exhibit the coexistence of two stable limit cycles, yet in a drastically different parameter range than the bichaotic one.

Instead of using p-doped silicon as our working electrode as in Refs. 33 and 34, we use n-doped silicon. The electro-oxidation reaction proceeds through the following net reaction:



where $1 \leq \lambda_{\text{VB}} \leq 4$ denotes the number of charge carriers that come from the valence band of the silicon. Since at least the first oxidation requires a valence band hole, the electro-oxidation of n-doped Si requires the illumination of the electrode with a wavelength that is larger than the bandgap. The illumination intensity is thus an additional bifurcation parameter in our study. The oxide formed in reaction (1) is chemically etched in the overall reaction,³⁵



The interaction between oxidation and etching kinetics is believed to cause the oscillatory behavior;³⁰ yet, the corresponding feedback loops could not be identified.

The rest of the article is structured as follows. In Sec. II, we introduce the experimental setup. In Sec. III, we first show the results obtained with one electrode, where birhythmicity is illustrated in the phase space, the physical space, and the frequency domain. Then, coupling experiments with two electrodes are presented. Implications of the experimental data concerning intrinsic and extrinsic coupling of the birhythmic system are discussed in Sec. IV.

II. EXPERIMENTAL SYSTEM

The experimental setup is sketched in Fig. 1. It consisted of a three electrode cell combined with an ellipsomicroscopic imaging setup and a laser illumination setup. The working electrode (WE) was an n-doped ($1\text{--}10\ \Omega\text{cm}$) Si (111) sample. We use an external resistor with a resistance such that $R_{\text{ext}}A = 1\ \text{k}\Omega\text{cm}^2$, connected in series with the WE to introduce a linear global coupling to our system; this tends to synchronize the electrode surface. For the measurements with two working electrodes, we placed two separate Si samples on one holder with two connecting wires, which were short-circuited before the external resistor. The electrolyte (500 ml)

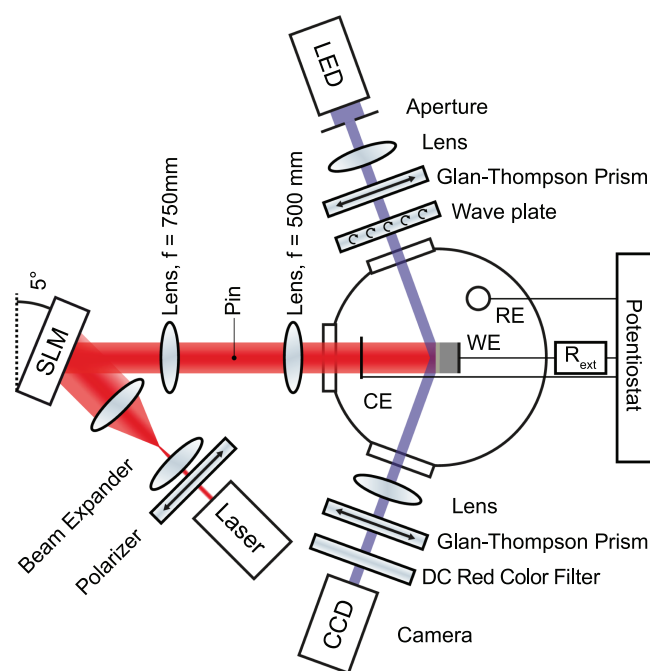


FIG. 1. Sketch of the experimental setup (not to scale) with its three parts: the laser illumination setup, with a spatial light modulator (SLM) as a centerpiece; the ellipsometric imaging setup, allowing spatially resolved *in situ* monitoring of the electrode surface; and the electrochemical setup, consisting of an electrochemical cell and a potentiostat. Note that we connected a resistor R_{ext} between the working electrode (WE) and the potentiostat.

consisted of 0.06 M NH_4F and 142 mM H_2SO_4 and was purged with argon and stirred throughout the measurements. We monitored the lateral uniformity of the electrode/electrolyte interface *in situ* by probing the relative change in the optical path length with the ellipsomicroscopic surface imaging setup.^{36,37} The resulting ellipsometric intensity signal ξ will be presented as a percentage of the saturation threshold of the recording camera. The laser illumination intensity at the electrode was controlled with a spatial light modulator (SLM) (Hamamatsu, X10468-06). The SLM ensured a uniform illumination intensity across the electrode, and when two electrodes were used, it enabled us to control the illumination intensity of each electrode separately, allowing for different initialization protocols. Further experimental details can be found in the [supplementary material](#).

III. RESULTS

In Fig. 2, exemplary time series of the current density j and the spatially averaged ellipsometric intensity signal (ξ) of the two oscillation types found during Si electrodisolution are depicted. The oscillations shown in Figs. 2(a) and 2(b) are HAOs, and the ones in Figs. 2(c) and 2(d) are LAOs. The most striking differences between the two oscillation types are that the HAOs have a larger amplitude of the current density and a higher frequency than the LAOs. They also differ in their shapes; specifically, the current of the HAOs is limited by the concentration of the available valence band holes during part of the oscillation. In Fig. 2(a), the current limit is indicated by a dotted line. We can tune this limit by changing the illumination intensity. Even though this means that the current amplitude of the HAO can be lower than the one of the LAO, we keep the naming convention introduced in the literature.³³

The two types of oscillations depicted in Fig. 2 were measured at identical parameter values, indicating that the system is birhythmic. Thus, which oscillation type is attained depends on the initial conditions. In order to establish HAOs, we performed a voltage

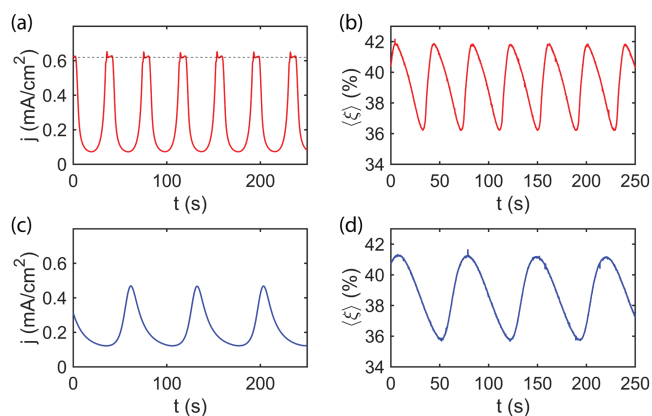


FIG. 2. Exemplary time series of a High Amplitude Oscillation (HAO), red, and of a Low Amplitude Oscillation (LAO), blue. (a) and (c) Current density j . (b) and (d) Spatially averaged ellipsometric intensity (ξ). Both oscillations were measured at $U = 6$ V vs MSE, $R_{\text{ext}}A = 1$ k Ω cm^2 , $A = 15.72$ mm^2 , and $I_{\text{ill}} = 1.31$ mW/cm^2 .

step from the open-circuit potential to a potential in the oscillatory region (6 V vs MSE for the measurements in Fig. 2) at a high illumination intensity (>2.5 mW/cm^2) and then reduced the illumination intensity to the desired intensity after the first two transient current oscillations. The LAOs were initialized by performing the same potential jump at the same high initial illumination intensity as when initializing the HAOs. However, before lowering the illumination intensity to the desired value, we waited until any transients had decayed. Below, we refer to these two protocols as the HAO- and the LAO-initialization protocols, respectively.

A. Parameter space

In the following, we determine the illumination intensity interval in which the system exhibits birhythmicity at 6 V vs MSE. Therefore, we first initialized HAOs at a low illumination intensity of 0.68 mW/cm^2 and then increased the illumination intensity stepwise. At each step, we waited until any transients had died out and then recorded the oscillation. In Fig. 3(a), representative HAOs at different illumination intensities are shown in the $j(\xi)$ -plane. In these phase portraits, the increase in the illumination-limited current plateau with increasing illumination density becomes obvious. When we increase the illumination intensity beyond the highest illumination intensity shown in Fig. 3(a), the system transitions to LAOs.

As we will detail below, the transition from HAOs to LAOs occurred through a nucleation and growth mechanism of the LAOs, which entailed very long (≥ 2 h), spatially inhomogeneous, transients. Therefore, we investigated the LAO branch by re-initializing LAOs according to the LAO-initialization protocol. In this way, we obtained spatially uniform oscillations before we lowered the illumination stepwise.

In Fig. 3(b), LAOs measured at the same parameters as in Fig. 3(a) are depicted. The LAOs remain spatially homogeneous until the illumination is lowered down to 1 mW/cm^2 . For lower illumination intensities, patterns emerge, leading to a lower amplitude of the spatially averaged signals, as shown in Fig. 3(b). The spatial symmetry breaking at a low illumination intensity confirms our previous findings.^{38,39} Comparing the location of the coexisting HAOs and LAOs in the phase-space projections in Figs. 3(a) and 3(b), it becomes obvious that they overlap at the corresponding illumination intensity. This strongly suggests that they live in an at least three dimensional phase space.

The hysteretic behavior is summarized in Fig. 3(c) where the average current densities of the oscillations are plotted vs the illumination intensity. Here, the measurement series shown in red was initialized using the HAO protocol, and the measurement series shown in blue was initialized using the LAO protocol, as described above. The HAO measurement series starts at low illumination intensities. If we follow it toward higher illumination intensities, we see that the average current density decreases with increasing illumination before reaching a fixed value at approximately 0.26 mA/cm^2 . The LAO measurement series starts at high illumination intensities. Following it, we see that the average current density does not change with decreasing illumination intensity until the system transitions from the LAO to the HAO at an illumination intensity of 0.72 mW/cm^2 .

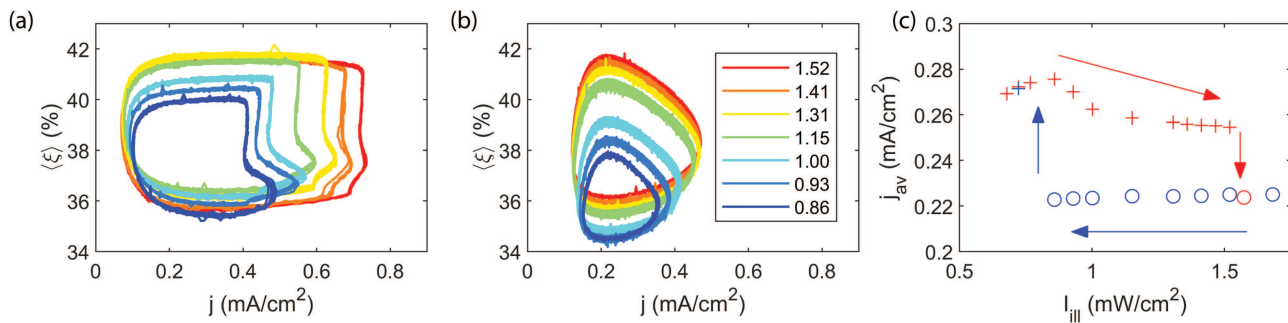


FIG. 3. Birhythmic oscillations in the $j(\xi)$ -plane: (a) HAOs and (b) LAOs at different illumination intensities I_{III} (mW/cm²) indicated by their respective color [see the legend in (b)]. Other parameter values: 6 V vs MSE and $R_{ext}A = 1 \text{ k}\Omega \text{ cm}^2$ with $A = 15.72 \text{ mm}^2$. (c) Average current density j_{av} of LAOs (\circ) and HAOs ($+$) vs illumination intensity I_{III} for the same parameters as used in (a) and (b). The measurements of (a) and (b) are included. The arrows indicate the order of measurement. Data from two separate measurement series: Red/blue symbols indicating that the series was initialized at low/high illumination intensities and that the illumination intensity was increased/decreased stepwise (see the text).

Next, we will have a closer look at the transient behavior during the transition from HAOs to LAOs at high illumination intensities and the transition from LAOs to HAOs at low illumination intensities.

A 1D cut vs time of the evolution of ξ and three 2D snapshots of the ellipsometric signal during the HAO→LAO transition are shown in Figs. 4(a) and 4(b) (Multimedia view). Shortly after having increased the illumination intensity, a nucleus of the LAO appeared in the lower left part of the electrode at a point in time where the HAO current was limited and thus very sensitive toward an increase in the hole concentration at the interface. This nucleus expands in space each time the HAO has again reached the current-limited phase. This indicates that the transition is triggered by diffusion of holes from the LAO region to the HAO region.

Thus, during the transition, the LAO state expands in a step-like manner resulting in a striped pattern on the electrode surface [Fig. 4(b)]. The stepwise expansion can also be seen from the checkerboard pattern in the 1D-cut taken approximately along the direction of propagation of the LAO region. The arrangement of the squares of the checkerboard pattern reflects that the ratio of the frequencies of HAOs and LAOs is approximately 2:1.

In contrast to this stepwise transition, the transition from a LAO to a HAO at the low illumination border is abrupt and takes place on the entire electrode at the same time. In Figs. 4(c) and 4(d) (Multimedia view), an example of such a transition is shown. Once the illumination has been reduced below a critical value, the electrode attains a HAO as soon as the current reaches the new maximal current level imposed by the reduced illumination.

If we expand our parameter space by also changing the applied voltage U , we obtain the 2D phase diagram shown in Fig. 5. Here, the HAOs are marked with crosses and the LAOs with circles. The red and blue areas indicate the regions where only HAOs and LAOs, respectively, were found, and the striped area marks the birhythmic region. Note that we only include measurements at the edges of and not within the birhythmic region for clarity. Evidently, the birhythmic region extends over a large region in this parameter plane, demonstrating that birhythmicity is a robust feature of the system.

B. Frequency domain

For a further characterization of the birhythmicity, it is instructive to investigate how the frequencies of HAOs and LAOs change as a function of the parameter and, in particular, how they behave at the transition points between the two oscillation forms. The easiest way to realize this is to perform a slow voltage scan while keeping the illumination intensity at a constant value. Therefore, we initialized the system at $I_{III} = 0.78 \text{ mW/cm}^2$ on either side of the birhythmic region and swept the voltage slowly until a transition was observed. Then, the voltage sweep was reversed, and the voltage was swept back to the initial value. We used a sweep rate of $dU/dt = 0.1 \text{ mV/s}$, which is slow on the time scale of the oscillations. Hence, we consider the measured quasi-stationary states to be a good representation of the true state at the respective voltages.

In Fig. 6, the resulting spectrograms of the spatially averaged ellipsometric intensity signal of two such scans are shown. Figure 6(a) depicts an experiment that we initialized in a LAO at a low voltage and 6(b) the one that we initialized in a HAO at high voltages. In each spectrogram, the main frequency and the second frequency at each voltage are marked with a solid line and a dashed line, respectively.

In the spectrogram in Fig. 6(a), we see that the main frequency of the initial LAO at 3.9 V vs MSE decreases before the system transitions to the faster oscillating HAO state at 5.8 V vs MSE. This transition from LAOs to HAOs occurs again quasi-simultaneously on the entire electrode, just as in the case when we varied the illumination, cf. Figs. 4(c) and 4(d). As the system undergoes a transition to a HAO, the main frequency abruptly jumps from 16 to 26 mHz. The frequency of the HAO first stays approximately constant and then starts to increase at about 5 V vs MSE. The increase in the frequency is accompanied by the emergence of a subharmonic mode.

We observe a similar behavior when the system is initialized in a HAO state and the voltage is swept toward lower values [Fig. 6(b)]. First, the frequency hardly changes with decreasing voltage until about 5 V vs MSE where it starts to increase and a first subharmonic peak emerges. In a small voltage interval around 4.5 V vs MSE,

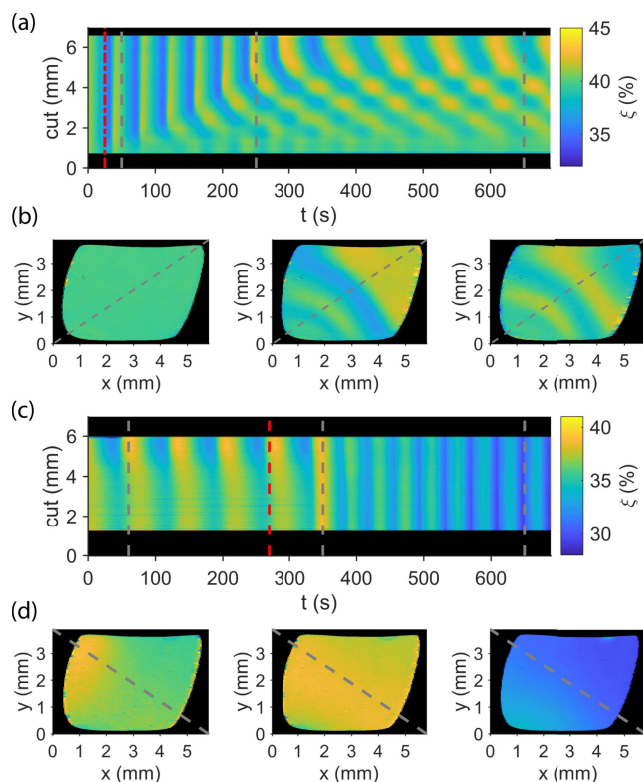


FIG. 4. Examples of the spatiotemporal dynamics at the border of the birhythmic region when the system transitions to the other oscillatory state: (a) and (b) high illumination (transition from HAO to LAO) and (c) and (d) low illumination (transition from LAO to HAO) at the same parameters as in Fig. 3(c). The dashed red lines indicate the time when the illumination intensity was changed. (a) and (c) Temporal evolution of the ellipsometric intensity of a 1D cut indicated by the dashed line in the snapshots in (b) and (d), respectively. (b) and (d) Snapshots of the ellipsometric intensity taken at the times indicated by the dashed gray lines in (a) and (c), respectively. $R_{\text{ext}}A = 1 \text{ k}\Omega \text{ cm}^2$ with $A = 15.72 \text{ mm}^2$. Multimedia views: <https://doi.org/10.1063/5.0064266.1>; <https://doi.org/10.1063/5.0064266.2>

this first subharmonic peak is accompanied by a sub-subharmonic frequency. The emergence of the subharmonic frequencies is accompanied by a spatial symmetry breaking, and the electrode tends to exhibit antiphase behavior. These phase-cluster-type patterns disappear again at lower potentials before the system transitions into the LAO state at 4 V vs MSE. Interestingly, at this transition, the subharmonic frequency of the HAO matches the main frequency of the LAO, and, accordingly, the main frequency of the HAO matches the first superharmonic frequency of the LAO. The appearance of the subharmonic frequency during the HAOs and the 1:2 frequency ratio of LAOs and HAOs at the HAO→LAO transition could be linked to a mutual influence of the two oscillations in the phase space. We will come back to this point below.

C. Two electrodes

To better understand how HAOs and LAOs influence each other, we will now look at what happens when we split the working

electrode into two smaller electrodes and couple them through a common external resistor. Due to this coupling, any change in current at one electrode causes the potential drops across both electrode/electrolyte interfaces $U_{\text{el},1/2}$ to change according to

$$U_{\text{el},1} = U_{\text{el},2} = U - R_{\text{ext}}(j_1A_1 + j_2A_2), \quad (3)$$

where U is the externally applied voltage and $j_{1/2}$ and $A_{1/2}$ are the current densities and areas of the respective electrodes. The use of the SLM allows us to employ different initialization protocols to the two electrodes so that we can initialize each electrode in either a HAO or a LAO state independently. In Fig. 7, the resulting time series of the spatially averaged ellipsometric intensity of the respective electrodes are shown for three different cases. All three cases were measured at the same parameters, and they only differ in the initialization protocol. Note that both electrodes remain essentially spatially homogeneous except the LAO initialized electrode of case (c) where minor spatial wave-like patterns emerged.

Figure 7(a) (Multimedia view) depicts time series of the two electrodes when they are both initialized with the HAO protocol. It can be seen that the oscillations on the two electrodes are slightly out of phase at $t = 0 \text{ s}$, are in phase at $t = 185 \text{ s}$, and have drifted to an antiphase configuration at $t = 550 \text{ s}$. Clearly, slightly different parameters of the two electrodes (such as a minor difference in their electrode areas) lead to a small difference of their natural frequencies, and the coupling via the external resistor does not suffice to synchronize them.

The picture is different in the case of the LAOs. When we initialize both electrodes using the LAO protocol, they typically exhibit phase synchronization, as can be seen in Fig. 7(b) (Multimedia view).

Figure 7(c) (Multimedia view) depicts an example where electrode 1 was initialized with the HAO protocol and electrode 2 with the LAO protocol. In this case, electrode 1 assumes a periodic HAO, which is very close to the one of case (a). In contrast, electrode 2 does

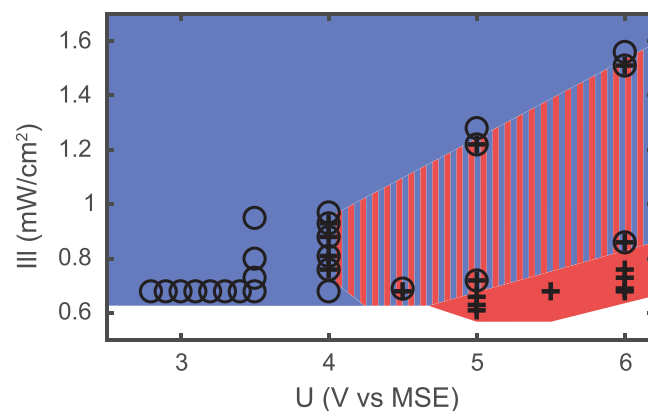


FIG. 5. Birhythmic parameter region in the U - I_{III} parameter plane: HAOs (+) and LAOs (○). Approximate existence region of HAOs (red) and LAOs (blue). The striped region indicates the birhythmic region where both oscillation types are found. For clarity, only the measurements at the edges are shown in the birhythmic region. All measurements with $R_{\text{ext}}A = 1 \text{ k}\Omega \text{ cm}^2$.

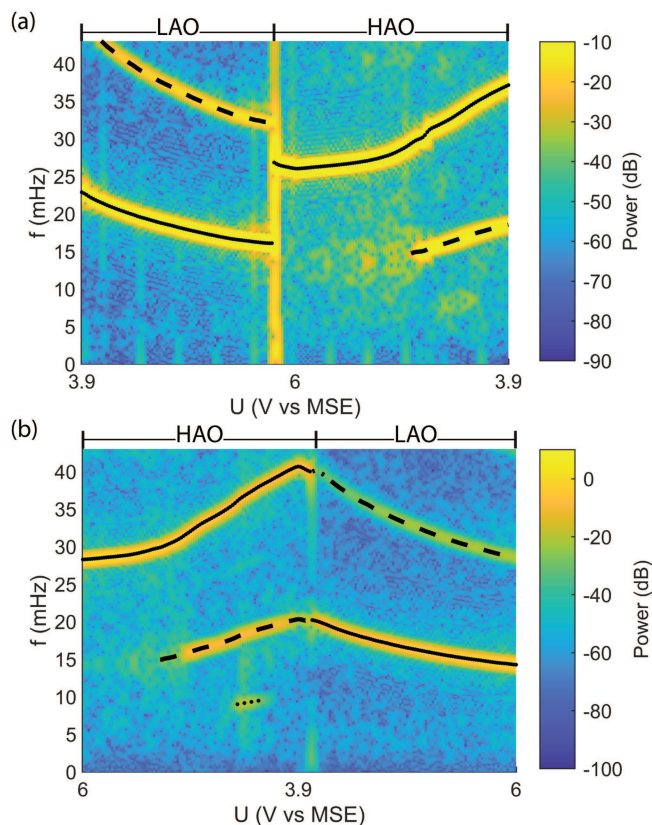


FIG. 6. Spectrogram of the spatially averaged ellipsometric intensity signal (ξ) from a quasi-stationary cyclic voltage scan ($dU/dt = 0.1$ mV/s) at illumination intensity $I_{\text{ill}} = 0.78$ mW/cm². The solid line indicates the main frequency, the dashed line indicates the second frequency, and the dotted line indicates the third frequency. (a) System initialized in a LAO state at 3.9 V vs MSE. (b) System initialized in a HAO state at 6 V vs MSE. Both measurements with $R_{\text{ext}}A = 1$ k Ω cm² and with $A = 17.51$ mm² in (a) and $A = 16.69$ mm² in (b).

not oscillate in a simple periodic LAO state. Alternatively, it exhibits a more complex temporal behavior. The frequency spectrum of the time series (not shown) exhibits a strongly enhanced background distribution around the main oscillation frequency, suggesting that the dynamics is chaotic.

This counterintuitive coexistence of chaos and order is not only stable under these exact conditions, but it persists for a wide range of potentials. When initializing the two electrodes in the same way as in Fig. 7(c) and then performing a quasi-static cyclic sweep of the applied potential, we obtain two spectrograms that are shown in Fig. 8.

Again, the sweep rate was slow ($dU/dt = 0.1$ mV/s) on the time scale of the oscillations, and we assume that the measured states are in good agreement with the true state at the respective parameters. Figure 8(a) shows the corresponding spectrogram of the electrode that was initialized with the HAO protocol. The electrode oscillates in a HAO state and behaves similarly to a single electrode under the same conditions; cf. Fig. 6(b). The only difference is that the subharmonic frequency is active in the entire existence region of the HAOs, not just from approximately 5 V vs MSE downward. Figure 8(b) shows the spectrogram of the electrode that was initialized according to the LAO protocol. This spectrogram differs significantly from the case with only one electrode; cf. LAO regions in Fig. 6. Here, we can see a broad potential region between 6 V vs MSE and approximately 4.9 V vs MSE, indicated by the dashed red line, where the power spectrum exhibits a strongly enhanced background and is smeared out around the main frequency and the first superharmonic frequency. This is a manifestation of the temporally complex behavior. Hence, we have a large region in the parameter space in which we find the coexistence of a periodic HAO on one electrode and complex, most likely chaotic oscillations on the other one. For potentials beyond the dashed red line, the spectrogram of electrode 2 becomes narrower again before the superharmonic frequency disappears at the same voltage at which electrode 1 transitions from the HAO to the LAO. In this intermediate region, the HAOs and LAOs on the two electrodes exhibit a 2:1 locking. After the transition of electrode 1 to the LAO state, both electrodes exhibit phase-synchronized LAOs. The reason for the slightly lower power after the transition is that patterns form on both electrodes, suppressing the amplitude

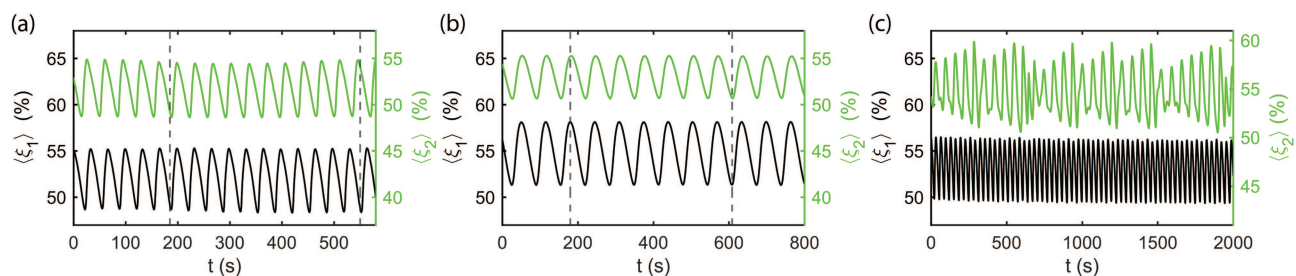


FIG. 7. Exemplary time series of the spatially averaged ellipsometric intensity of two electrodes coupled electrically through an external resistor. (a) Both electrode 1 (ξ_1) and electrode 2 (ξ_2) in a HAO state. (b) Both electrodes in a LAO state. (c) Electrode 1 in a HAO state and electrode 2 in a chaotic state. Here, electrode 2 was initialized using the LAO-initialization protocol. $A_1 = 11.43$ mm², $A_2 = 10.55$ mm². $R_{\text{ext}}(A_1 + A_2) = 1$ k Ω cm², $I_{\text{ill}} = 1.0$ mW/cm², $U = 5.75$ V vs MSE. Multimedia views: <https://doi.org/10.1063/5.0064266.3>; <https://doi.org/10.1063/5.0064266.4>; <https://doi.org/10.1063/5.0064266.5>

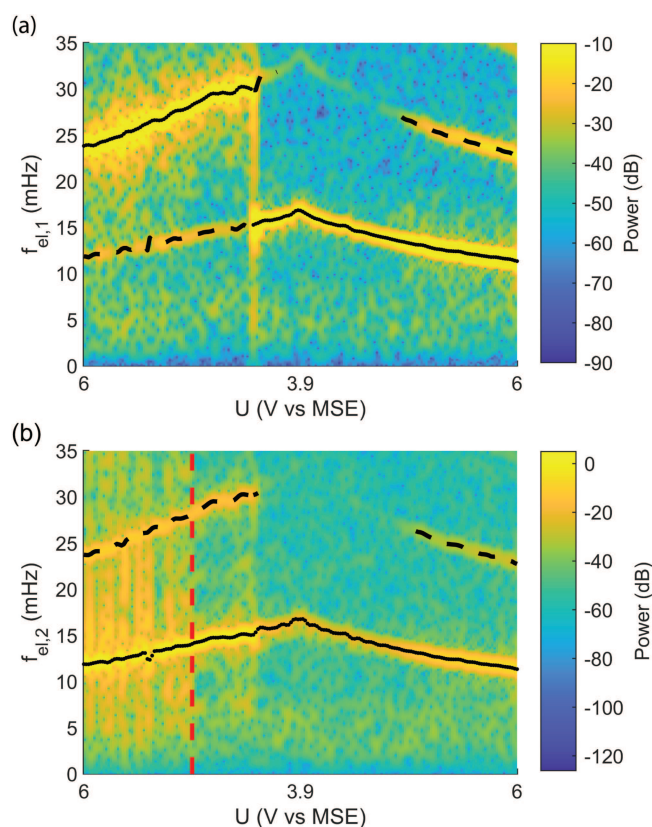


FIG. 8. Spectrograms of two coupled electrodes, obtained from the spatially averaged ellipsometric intensity signal and a quasi-stationary cyclic voltage scan ($dU/dt = 0.1$ mV/s) at illumination intensity $I_{\text{ill}} = 0.94$ mW/cm² and $R_{\text{ext}} (A_1 + A_2) = 1$ k Ω cm². The solid line indicates the main frequency, and the dashed line indicates the second frequency. (a) Electrode 1, initialized with the HAO protocol, $A_1 = 5.53$ mm². (b) Electrode 2, initialized with the LAO protocol, $A_2 = 6.17$ mm².

of the spatially averaged signal. Once the electrodes become spatially more uniform again, the superharmonic peak in the spectrum becomes visible again, too.

IV. DISCUSSION

We presented clear-cut experimental evidence that the electrodisolution of silicon in a fluoride-containing electrolyte exhibits birhythmicity. Besides this observation, our experiments elucidated unusual, though general ways, in which coexisting limit cycles can interact with each other. In the following, we take a closer look at these interactions. We discriminate here between an *extrinsic* interaction of (nearly) identical birhythmic systems and an *intrinsic* interaction of the two limit cycles in the phase space.

The extrinsic coupling mechanism is the one that is easier to rationalize. We will, therefore, discuss it first. Consider again the results depicted in Fig. 7. Here, we coupled two nearly identical Si electrodes through an external resistor. Hence, the coupling acts, as

obvious from Eq. (3), on the potential drops across the interface of the electrodes. The facts that the oscillations of the two electrodes phase-synchronize when they are both initialized with the LAO protocol but that the phases of the oscillations remain drifting when the electrodes are initialized with the HAO protocol reveal that the sensitivity of HAOs and LAOs toward perturbations in the potential is vastly different. The experiment, where the two electrodes were initialized in different states, shows that the impact of the electrode initialized in an LAO on the one initialized in an HAO is negligible, while the other way round, the dynamics of the LAO initialized electrode is strongly forced by the electrode in the HAO state. Thus, the mutual interactions of the two types of oscillations are *unidirectional*, i.e., of the master–slave type.

The phase-space portraits depicted in Fig. 3 shed light on this unidirectional coupling. The phase portraits of the two limit cycles intersect in the $j(\xi)$ -phase-space plane, suggesting that the oscillations live in a phase space spanned by at least three essential variables. The sensitivity of the LAO with respect to changes in the electrode potential indicates that the electrode potential is an essential variable for the LAOs. Contrarily, from the insensitivity of the HAOs upon variations of the electrode potential, we can conjecture that the HAO limit cycle occupies a subspace of the phase space that is orthogonal to the electrode potential axis. Yet, since, during HAOs, the current oscillates, the coupling through the resistor changes the electrode potential of both electrodes. The oscillating electrode potential acts like a periodic forcing on the LAO, while it is like an “invariant” parameter for the HAO.

The coupling experiments presented in Fig. 7 were carried out at 5.75 V vs MSE. The spectrograms in Fig. 6 confirm that approximately between 6 and 5 V vs MSE, the HAO frequency is essentially independent of the applied voltage.

This changes at lower voltages, where we will argue that an intrinsic coupling comes into play. Here, the HAO frequency increases considerably, and, more strikingly, a subharmonic frequency emerges. The corresponding time series of the current and average ellipsometric signal exhibit the typical signature of a period doubling bifurcation, i.e., increasing differences in the maxima and minima of successive oscillations with decreasing voltage. This corroborates that the system lives in at least a three-dimensional phase space. More importantly, the subharmonic frequency coincides almost perfectly with the frequency of the LAO, at least at the HAO→LAO transition [see Fig. 6(b)]. It appears likely that this is not a coincidence but rather that the existence of the LAO in the phase space triggers the period doubling bifurcation. In other words, the HAO is intrinsically entrained to the LAOs in a 2:1 resonance.

A possible scenario would be as follows: Recall that also here, the working electrode is connected to the potentiostat via an external resistor. Thus, the oscillating current during HAOs causes an oscillating electrode potential. Above, we have discussed that these changes in the electrode potential affect the LAOs in a second electrode. For an individual electrode, the LAOs exist somewhere else in the phase space. Yet, the phase-space structure can be such that the oscillatory motion of the LAO is felt also on the other side of the separatrix where initial conditions relax to the HAO. Hence, the oscillatory potential will induce an oscillatory motion in the plane spanned by the essential variables of the LAOs. We have argued above that one of these variables is the electrode potential upon

which the HAOs are insensitive. HAOs could, however, be sensitive to changes in the second essential LAO variable. Then, we can interpret the period doubling of the HAO as being caused by an intrinsic entrainment originating from the coexisting LAOs.

Note that in addition, at voltages lower than approximately 4 V vs MSE, the HAOs might become more sensitive against perturbations in the electrode potential than they are at higher potentials. We have seen that the LAOs are sensitive toward the concentration of holes at the Si/SiO₂ interface. At high voltages, the potential drop across the space charge layer is large, and with the space charge layer being compact nearly all holes that are generated by the illumination in the bulk of the Si are quickly drawn to the Si/SiO₂ interface. Their concentration thus remains unaffected by the externally applied voltage. At lower voltages, however, some of the holes will recombine with electrons before reaching the surface. The lower the voltage, the larger the fraction of holes that is lost due to recombination. At present, we do not know whether the mechanism leads to an appreciable change in the hole concentration at the interface. If it does, it would lead to a sensitivity change of the HAOs toward changes in the potential. However, independently of the sensitivity of the HAOs toward perturbations in the electrode potential, the occurrence of a 2:1 resonance still seems to require that the HAOs couple to the motion of the LAOs—most likely involving a second variable.

The different sensitivity of HAOs and LAOs on perturbations in different variables also explains the different nature of the transitions HAO→LAO and LAO→HAO (cf. Fig. 4).

Let us first look at the HAO→LAO transition, which occurs through a nucleation and growth mechanism. We can assume that the growth of the LAO domain is mediated via diffusion of valence band holes. Every time the HAO is on the current-limited plateau, diffusion of holes from the LAO covered region to the HAO region triggers a transition from the HAO to the LAO close to the boundary between the two oscillations. Thus, the propagation velocity of the LAO region is determined by a combination of the limited (non-local, see Refs. 38 and 39) diffusion length of the holes and the oscillation frequency of the HAOs.

In contrast, the LAO→HAO transition takes place on the entire electrode at almost exactly the same time. This fast transition indicates that the coupling has a nearly global range. Considering that the external resistor introduces a global coupling on the potential and the fact that the LAOs are very sensitive to changes in the potential, it is most likely that this spatially uniform transition is triggered through a perturbation in the potential that lifts the LAO on the entire electrode across the separatrix.

Finally, let us turn again to the two coupled electrodes, where one electrode was initiated in the HAO state and the other in the LAO state [Fig. 7(c)]. These dynamics are very similar to the smallest chimera state as found as solutions in a chemical model of two coupled identical unimodal oscillators.^{40,41} Similar to our results, the simulation shows one oscillator exhibiting regular oscillations, while the other one exhibited chaotic oscillations. To the best of our knowledge, we present here the first experimental realization of a smallest chimera state consisting of only two coupled oscillators. Furthermore, the authors of Refs. 40 and 41 attributed this particular type of chimera state to a master-slave-type coupling. The authors argue that in their case, this coupling was generated by a

canard explosion. We present evidence that in our case, the effective unidirectional coupling comes about by the widely different sensitivities of the two birhythmic limit cycles with respect to the coupling variables.

Yet, we note that at this stage, it is unclear whether the chaotic behavior of the LAO initialized electrode can be fully explained by the unidirectional coupling. The dynamics is further complicated by the fact that the forcing of the LAO by the HAO increases the maximal current density of the LAO such that it reaches the illumination-limited current level. It has been shown that when an LAO comes close to the illumination-limited current level, the electrode tends to form spatial structures.^{38,39} Here, too, the electrode does not remain completely uniform but tends to form fast spreading waves. We also note that the chaotic behavior exists only in the voltage interval between 6 and 5 V vs MSE, as indicated by the red-dashed line in Fig. 8(b). For lower voltages, the oscillations initialized with the LAO protocol exhibit a 1:2 locking to the HAO until the HAOs transition to LAOs at about 4.3 V vs MSE.

A connection between birhythmic systems and chimera states has also been discussed in the context of ensembles of coupled oscillators.^{26,27} Reference 27 considered a model of nonlocally coupled birhythmic oscillators and found that the oscillators could organize themselves in synchronized domains separated by asynchronous domains. Also, in ensembles of birhythmic Stuart-Landau-type as well as phase oscillators, chimera states were reported to exist.²⁶

With the present system, it might be possible to experimentally validate some of these theoretical studies. Furthermore, when changing the perspective and viewing the system of two coupled electrodes not as a system consisting of two individual units but instead regarding each subsystem as an oscillatory medium with many coupled degrees of freedom, then a large variety of possibilities opens up to investigate pattern formation in coupled networks experimentally.

V. CONCLUSION

In this study, we confirmed that there are two different types of current oscillations during silicon electrodisolution. We explicitly showed that, for a broad range of parameters, these oscillation types are bistable; i.e., the system exhibits birhythmicity. Furthermore, we were able to identify three dynamical properties that are closely related to the birhythmic nature of the system: (1) An *intrinsic* entrainment of the motion of one oscillator to the motion of the other one, mediated by the vector field in the phase space. (2) A unidirectional or master-slave-type coupling of two identical oscillatory systems. This behavior is linked to the possibility that the two limit cycles exhibit pronouncedly different sensitivities toward the perturbation in a variable. (3) The existence of a stable state of two coupled, identical electrodes where one electrode oscillated chaotically and the other one periodically, illustrating a route to a two oscillator minimal chimera state.

Currently, we are only in the beginning of understanding coupled birhythmic systems. The present system promises to become a prototypical experimental model system for studies of birhythmic dynamics. The very property that distinguishes the present system

from other ones is that the initial conditions can be easily controlled both in time and space, allowing to set each location—or a coupled electrode—in the chosen oscillation type.

SUPPLEMENTARY MATERIAL

See the [supplementary material](#) for a detailed explanation of the experimental setup.

AUTHORS' CONTRIBUTIONS

J.C.W. and M.P. contributed equally to this work.

ACKNOWLEDGMENTS

The authors thank Sindre W. Haugland and Munir M. Salman for fruitful discussions and are grateful to Richard Hueck for his preliminary experimental work and to Anton Tosolini for his help with the installation of the spatial light modulator. This project was funded by the Deutsche Forschungsgemeinschaft (DFG, German Research Foundation) project (No. KR1189/18) "Chimera States and Beyond."

DATA AVAILABILITY

The data that support the findings of this study are available from the corresponding author upon reasonable request.

REFERENCES

- 1A. N. Pisarchik and U. Feudel, "Control of multistability," *Phys. Rep.* **540**, 167–218 (2014).
- 2O. Decroly and A. Goldbeter, "Birhythmicity, chaos, and other patterns of temporal self-organization in a multiply regulated biochemical system," *Proc. Natl. Acad. Sci. U.S.A.* **79**, 6917–6921 (1982).
- 3A. S. Mikhailov, *Foundations of Synergetics I: Distributed Active Systems*, Springer Series in Synergetics Vol. 51 (Springer, Berlin, 1994).
- 4D. S. Cohen and J. P. Keener, "Multiplicity and stability of oscillatory states in a continuous stirred tank reactor with exothermic consecutive reactions $A \rightarrow B \rightarrow C$," *Chem. Eng. Sci.* **31**, 115–122 (1976).
- 5F. T. Arecchi, R. Meucci, G. Puccioni, and J. Tredicce, "Experimental evidence of subharmonic bifurcations, multistability, and turbulence in a q-switched gas laser," *Phys. Rev. Lett.* **49**, 1217–1220 (1982).
- 6M. Alamgir and I. R. Epstein, "Birhythmicity and compound oscillation in coupled chemical oscillators: Chlorite-bromate-iodide system," *J. Am. Chem. Soc.* **105**, 2500–2502 (1983).
- 7M. Alamgir and I. R. Epstein, "Systematic design of chemical oscillators. Part 19. Experimental study of complex dynamical behavior in coupled chemical oscillators," *J. Phys. Chem.* **88**, 2848–2851 (1984).
- 8D. Biswas, T. Banerjee, and J. Kurths, "Control of birhythmicity through conjugate self-feedback: Theory and experiment," *Phys. Rev. E* **94**, 042226 (2016).
- 9J.-C. Roux, "Experimental studies of bifurcations leading to chaos in the Belousov-Zhabotinsky reaction," *Physica D* **7**, 57–68 (1983).
- 10P. Lamba and J. L. Hudson, "Experimental evidence of multiple oscillatory states in a continuous reactor," *Chem. Eng. Commun.* **32**, 369–375 (2007).
- 11J. Maselko and H. L. Swinney, "Complex periodic oscillations and Farey arithmetic in the Belousov-Zhabotinskii reaction," *J. Chem. Phys.* **85**, 6430–6441 (1986).
- 12B. Gray and J. Jones, "The heat release rates and cool flames of acetaldehyde oxidation in a continuously stirred tank reactor," *Combust. Flame* **57**, 3–14 (1984).
- 13D. Baulch, J. F. Griffiths, A. J. Pappin, and A. F. Sykes, "Stationary-state and oscillatory combustion of hydrogen in a well-stirred flow reactor," *Combust. Flame* **73**, 163–185 (1988).
- 14B. R. Johnson, J. F. Griffiths, and S. K. Scott, "Characterisation of oscillations in the $H_2 + O_2$ reaction in a continuous-flow reactor," *J. Chem. Soc., Faraday Trans.* **87**, 523–533 (1991).
- 15H. A. Lechner, D. A. Baxter, J. W. Clark, and J. H. Byrne, "Bistability and its regulation by serotonin in the endogenously bursting neuron R15 in Aplysia," *J. Neurophysiol.* **75**, 957–962 (1996).
- 16H. Jahnsen and R. Llinás, "Ionic basis for the electro-responsiveness and oscillatory properties of guinea-pig thalamic neurones *in vitro*," *J. Physiol.* **349**, 227–247 (1984).
- 17J. Hounsgaard, H. Hultborn, B. Jespersen, and O. Kiehn, "Bistability of alpha-motoneurons in the decerebrate cat and in the acute spinal cat after intravenous 5-hydroxytryptophan," *J. Physiol.* **405**, 345–367 (1988).
- 18J. S. Pendergast, K. D. Niswender, and S. Yamazaki, "The complex relationship between the light-entrainable and methamphetamine-sensitive circadian oscillators: Evidence from behavioral studies of period-mutant mice," *Eur. J. Neurosci.* **38**, 3044–3053 (2013).
- 19T. Nagy, E. Verner, V. Gáspár, H. Kori, and I. Z. Kiss, "Delayed feedback induced multirhythmicity in the oscillatory electrodisolution of copper," *Chaos* **25**, 064608 (2015).
- 20D. Battogtokh and J. J. Tyson, "Turbulence near cyclic fold bifurcations in birhythmic media," *Phys. Rev. E* **70**, 026212 (2004).
- 21M. Stich, M. Ipsen, and A. S. Mikhailov, "Self-organized stable pacemakers near the onset of birhythmicity," *Phys. Rev. Lett.* **86**, 4406–4409 (2001).
- 22M. Stich, M. Ipsen, and A. S. Mikhailov, "Self-organized pacemakers in birhythmic media," *Physica D* **171**, 19–40 (2002).
- 23R. Yamapi, G. Filatrella, and M. A. Aziz-Alaoui, "Global stability analysis of birhythmicity in a self-sustained oscillator," *Chaos* **20**, 013114 (2010).
- 24D. Biswas, T. Banerjee, and J. Kurths, "Control of birhythmicity: A self-feedback approach," *Chaos* **27**, 063110 (2017).
- 25O. V. Astakhov, S. V. Astakhov, N. S. Krakhovskaya, V. V. Astakhov, and J. Kurths, "The emergence of multistability and chaos in a two-mode van der Pol generator versus different connection types of linear oscillators," *Chaos* **28**, 063118 (2018).
- 26A. Yeldesbay, A. Pikovsky, and M. Rosenblum, "Chimeralike states in an ensemble of globally coupled oscillators," *Phys. Rev. Lett.* **112**, 144103 (2014).
- 27A. Provata, "Chimera states formed via a two-level synchronization mechanism," *J. Phys. Complex.* **1**, 025006 (2020).
- 28D. R. Turner, "Electropolishing silicon in hydrofluoric acid solutions," *J. Electrochem. Soc.* **105**, 402 (1958).
- 29V. Lehmann, "The physics of macropore formation in low doped n-type silicon," *J. Electrochem. Soc.* **140**, 2836 (1993).
- 30X. G. Zhang, *Electrochemistry of Silicon and Its Oxide* (Kluwer Academic Publishers, Boston, MA, 2004).
- 31K. Schönleber, C. Zensen, A. Heinrich, and K. Krischer, "Pattern formation during the oscillatory photoelectrodisolution of n-type silicon: Turbulence, clusters and chimeras," *New J. Phys.* **16**, 063024 (2014).
- 32L. Schmidt, K. Schönleber, K. Krischer, and V. García-Morales, "Coexistence of synchrony and incoherence in oscillatory media under nonlinear global coupling," *Chaos* **24**, 013102 (2014).
- 33K. Schönleber and K. Krischer, "High-amplitude versus low-amplitude current oscillations during the anodic oxidation of p-type silicon in fluoride containing electrolytes," *ChemPhysChem* **13**, 2989–2996 (2012).
- 34A. Tosolini, M. Patzauer, and K. Krischer, "Bichaoticity induced by inherent birhythmicity during the oscillatory electrodisolution of silicon," *Chaos* **29**, 043127 (2019).
- 35S. Cattarin, I. Frateur, M. Musiani, and B. Tribollet, "Electrodisolution of p-Si in acidic fluoride media modeling of the steady state," *J. Electrochem. Soc.* **147**, 3277 (2000).
- 36H. Rothermund, G. Haas, R. U. Franz, R. M. Tromp, and G. Ertl, "Imaging pattern formation in surface reactions from ultrahigh vacuum up to atmospheric pressures," *Science* **270**, 608–610 (1995).
- 37I. Miethe, V. García-Morales, and K. Krischer, "Irregular subharmonic cluster patterns in an autonomous photoelectrochemical oscillator," *Phys. Rev. Lett.* **102**, 194101 (2009).

³⁸M. Patzauer, R. Hueck, A. Tosolini, K. Schönleber, and K. Krischer, “Autonomous oscillations and pattern formation with zero external resistance during silicon electrodisolution,” *Electrochim. Acta* **246**, 315–321 (2017).

³⁹M. Patzauer and K. Krischer, “Self-organized multifrequency clusters in an oscillating electrochemical system with strong nonlinear coupling,” *Phys. Rev. Lett.* **126**, 194101 (2021).

⁴⁰N. M. Awal, D. Bullara, and I. R. Epstein, “The smallest chimera: Periodicity and chaos in a pair of coupled chemical oscillators,” *Chaos* **29**, 013131 (2019).

⁴¹N. M. Awal and I. R. Epstein, “Post-canard symmetry breaking and other exotic dynamic behaviors in identical coupled chemical oscillators,” *Phys. Rev. E* **101**, 042222 (2020).